Solid State Reaction of Serpentinite Mg$_3$Si$_2$O$_5$(OH)$_4$ with NaOH to Produce a New Basic Catalytic Phase Na$_2$Mg$_2$Si$_2$O$_7$ for Biodiesel Production

Gilvan M. Paz,[a,b] Sara S. Vieira,[a] Alexandre C. Bertoli,[a] Fabiane C. Ballotin,[a]
Edmilson M. de Moura,[c] Ana Paula C. Teixeira,[a] Demétrio A. S. Costa,[a]
Ottávio Carmignano[d] and Rochel M. Lago*,[a]

[a]Departamento de Química, Instituto de Ciências Exatas, Universidade Federal de Minas Gerais,
31270-901 Belo Horizonte-MG, Brazil

[b]Instituto Federal de Educação, Ciência e Tecnologia do Piauí, 64053-390 Teresina-PI, Brazil

[c]Departamento de Química, Centro de Ciências da Natureza, Universidade Federal do Piauí,
64049-550 Teresina-PI, Brazil

[d]Doutorado Inovação/Mineradora Pedras Congonhas, Universidade Federal de Minas Gerais,
31270-901 Belo Horizonte-MG, Brazil

Solid state reaction of serpentinite Mg$_3$Si$_2$O$_5$(OH)$_4$ with NaOH was investigated to produce new NaMgSi oxide phases with basic properties for application in catalysis. X-ray powder diffraction (XRD) showed that NaOH impregnated on serpentinite, specially 20% sodium and treated at 700 °C (20Na$_{700}$), led to the formation of a new crystalline phase Na$_2$Mg$_2$Si$_2$O$_7$. This solid state reaction is discussed in terms of a first step involving Na$^+$ diffusion and intercalation in the interlayer space of the serpentinite structure followed by a dihydroxylation and formation of the NaMgSi oxides. Temperature programmed reaction and desorption experiments with 20Na$_{700}$ combined with XRD suggested a strong basicity with high CO$_2$ uptake likely due to diffusion and interaction with the basic sites in the material structure. These materials were tested as catalysts for the transesterification of soybean oil with methanol. The obtained results are discussed in terms of a basic site Si–O$^-$Na$^+$ present in the in the Na$_2$Mg$_2$Si$_2$O$_7$ structure.

Keywords: serpentinite, sodium silicate, biodiesel, basic catalyst

Introduction

Serpentinite is a mineral family of hydrated magnesium silicates with formula Mg$_3$Si$_2$O$_5$(OH)$_4$ with 32-38% MgO, 35-40% SiO$_2$ and 12-13% H$_2$O, in addition to small amounts of Fe, Al, Cr and Ni.[1] Serpentinite is arranged in layers of 1:1 type[2] consisting of octahedral sheets of MgO$_2$(OH)$_4$ bound to tetrahedral sheets of SiO$_4$.[3,4]
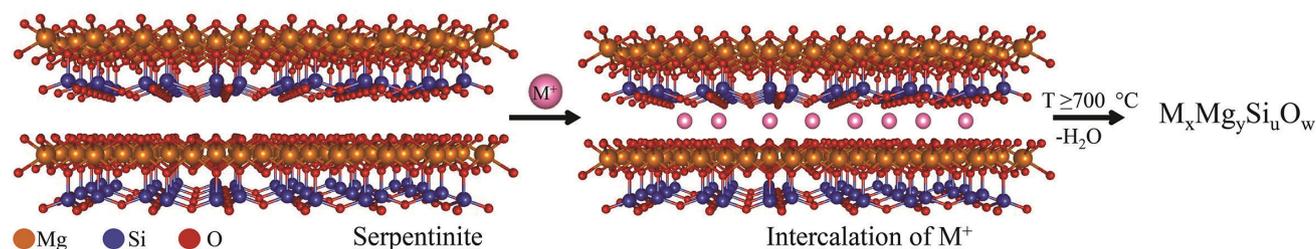
A previous work showed that serpentinite can react with K$^+$ to produce a new phase, K$_2$MgSiO$_4$, under relatively mild conditions.[5] On the other hand, chrysotile with the same chemical composition Mg$_3$Si$_2$O$_5$(OH)$_4$, but with a different structure, did not produce this phase.[6]

The layered serpentinite structure (lizardite) has a very interesting feature, which is the possibility of cations diffusion into the interlayer space followed by a solid state reaction to produce different MgSi oxide phases in relatively mild conditions, e.g., ca. 500 °C (Figure 1). On the other hand, the same phase K$_2$MgSiO$_4$ can also be prepared in a classical solid state reaction mixing K$_2$CO$_3$, SiO$_2$ and MgO, but at much higher temperatures, e.g., 1200 °C.[7,8]

Therefore, the intercalation of metal cations in serpentinite is potentially versatile mild route to prepare different metal MgSi oxides for a variety of applications. For example, the K$_2$MgSiO$_4$ phase showed basic properties and promising results as heterogeneous catalysts for different reactions such as isomerization of hexoses[9] and transesterification.[5,10] MSiMg oxides with Ce^{3+} or Tb^{3+} (M$_x$Sr$_2$MgSi$_2$O$_7$),[8] zinc magnesium silicate (Zn$_x$Mg$_{2-x}$SiO$_4$),[11] Ni/MgSiO$_3$ doped with alkaline earth,[12] Li$_2$MgSiO$_4$,[13] Ca$_2$MgSi$_2$O$_7$,[14] and Ce^{3+} and Eu^{2+} activated Ca$_7$Mg(SiO$_4$)$_4$ [15] also showed very interesting properties such as ceramics, insulators, catalysts, adsorbents, luminescent and others.

*e-mail: rochel@ufmg.br

Figure 1. Diffusion of metal cations into serpentinite (lizardite) interlayer space followed by a dehydration to form MSiMg oxides.

Heterogeneous basic catalysts for biodiesel synthesis have been intensively investigated in the last years such as alkaline and earth alkaline oxides,[16-18] transition metal oxides and rare earths (Mg/La and Al/La,[19] Zn/La,[20] Na$_2$ZrO$_3$),[21] zeolites and mesoporous silicas (NaX,[22] zeolites X and Y,[23] Na$_2$O/NaX,[24] SBA-15),[25] hydrotalcites[26,27] and some minerals (Ca$_2$MgSi$_2$O$_7$,[14] combination of chrysotile with KOH[6] and combinations of serpentinite with KOH).[5] Hereon, it is investigated the use of serpentinite as an available and low cost precursor to produce the unique Na$_2$Mg$_2$Si$_2$O$_7$ phase used for the first time as basic catalyst for biodiesel production.

Experimental

The serpentinite used in this work was provided by Pedras Congonhas Ltda. The samples, retained in 200 mesh sieves, were impregnated with aqueous NaOH in proportions of 5, 10 and 20% by weight of sodium (Na$^+$). The impregnation was done in a beaker, on a heating plate and magnetic stirring, at 80 °C. The materials were oven dried for 24 h at 80 °C to ensure complete drying and calcined at a heating rate of 10 °C min^{-1} in a horizontal tubular oven at 500, 700 or 900 °C for 3 h under an atmosphere of air. The impregnation of serpentinite was repeated according to the procedure described by Ballotin *et al.*[5] These samples are named hereon according to the Na$^+$ content and temperature treatment, for instance 20Na$_{700}$ contains 20 wt.% Na$^+$ treated at 700 °C.

The structural characterization was performed by X-ray powder diffraction (XRD) on a Shimadzu diffractometer, model XRD-7000 with CuKα (1.5406 Å) and scanning speed of 4° min^{-1}. The chemical composition was determined by fluorescence spectroscopy (FRX) on a Shimadzu EDX-720 vacuum spectrometer.

Thermogravimetric analyzes were performed on a Shimadzu DTG 60H equipment with synthetic air flow (50 mL min^{-1}), temperature range of 30-1000 °C and heating rate of 10 °C min^{-1}. In order to determine the basic properties of the material 20Na$_{700}$, a simultaneous thermogravimetric analysis mass spectrometry (TG-MS) analysis was applied. The base peak (*m/z* 44) was selected

to be monitored in a Netzsch TG/STA equipment coupled with Aelos spectrometer, model 7.0. The catalysts were previously treated in argon atmosphere (20 mL min^{-1}) at 500 °C for 1 h, followed by treatment at 50 °C under CO$_2$ flow (20 mL min^{-1}) for 1 h. Then, the material was heated to 1000 °C in argon at a rate of 5 °C min^{-1}. The measurements of Raman spectroscopy were performed on a Raman Senterra spectrometer from Bruker with a coupled optic microscope (Olympus BX51). The sample was excited using the laser at wavelength 633 nm, with a power of 0.2 mW. The number of settings was 10 and the integration time was 10 s.

Scanning electron microscopy (SEM) measurements were obtained on a Quanta 200-FEG 3D-FEI equipment. The specific surface areas (Brunauer-Emmett-Teller, BET) of the samples were analyzed by adsorption of N$_2$ at 77 K using the Autosorb1-MP Quantachrome equipment. Samples were degassed at 200 °C for 24 h prior to analysis.
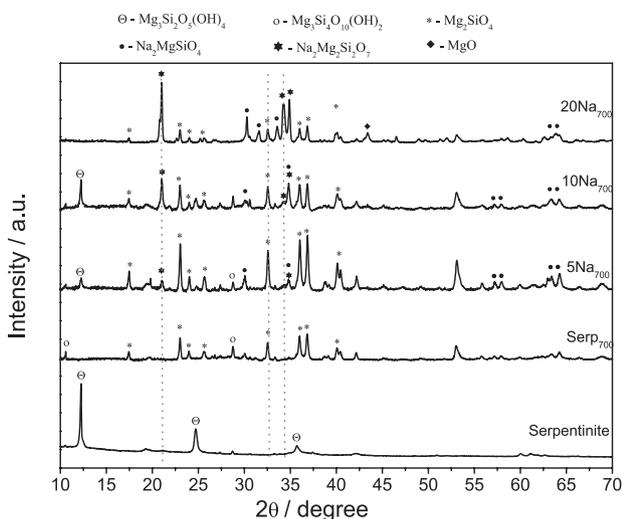
Biodiesel was synthesized using typical conditions found in the literature.[5] The reactions were carried out in a glass batch reactor at 60 and 100 °C under continuous stirring for 3 h with sample collection and analysis every 30 min. The molar ratios of oil:methanol used were 1:6, 1:9 and 1:12. The catalyst concentration in the reaction was 1, 5 and 10 wt.% in relation to oil. The reuse tests were carried out under the optimal reaction conditions established by experiments with fresh catalysts. After the reaction, the liquid phase was separated from the catalysts, and the recycling experiments were done by simple reuse of the catalysts without any treatment. Leaching was evaluated at the molar ratio of 1:9, using 5% catalyst. For the tests, the catalyst was transferred to the reaction medium containing only methanol. The system was maintained under constant stirring for 30 min at 60 or 100 °C. After this period, methanol was removed and transferred to a vial containing only soybean oil, thus proceeding with the reaction.

The methyl ester content was analyzed by gas chromatography coupled with flame ionization detector (GC-FID) using a Shimadzu QP apparatus 2010, equipped with Rtx-Wax capillary column (30 m, 25 mm and internal diameter of 0.25 µm).
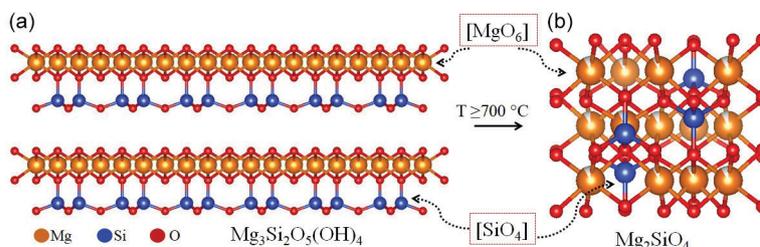
Results and Discussion

The serpentinite used in this work shows an approximate composition of 40% SiO_2 and 30% MgO, 10% Fe_2O_3 and small concentrations of Al, Ca, Ni and Mn. The thermogravimetric profile (Supplementary Information (SI) section) showed that serpentinite decomposes between 500-800 °C with a main weight loss of 8-9% related to the dehydroxylation of $Mg_3Si_2O_5(OH)_4$.

The main phases produced in this decomposition are magnesium silicates, e.g., forsterite (Mg_2SiO_4 JCDPS 4-769) as observed by X-ray diffraction (Figure 2). Peaks at 2θ such as 9.5 and 28.6° also suggest the formation of another Mg silicate $Mg_3Si_4O_{10}(OH)_2$ (JCDPS 13-558). Equation 1 represents a simplified serpentinite decomposition process to form forsterite.

$$Mg_3Si_2O_5(OH)_4 \rightarrow Mg_2SiO_{4(forsterite)}/MgO/SiO_2 + 2H_2O \quad (1)$$

Figure 2. X-ray diffraction patterns of serpentinite samples, $Serp_{700}$ and $5Na_{700}$, $10Na_{700}$ and $20Na_{700}$.

Figure 3 shows the crystalline structures for both serpentinite and forsterite. The serpentinite crystallizes as a triclinic system with space group P_1 based on layers (100) of [SiO_4] tetrahedra and [MgO_6] octahedra layer connected by two [SiO_4] tetrahedra to form [Si_2O_7] (Figure 3a).
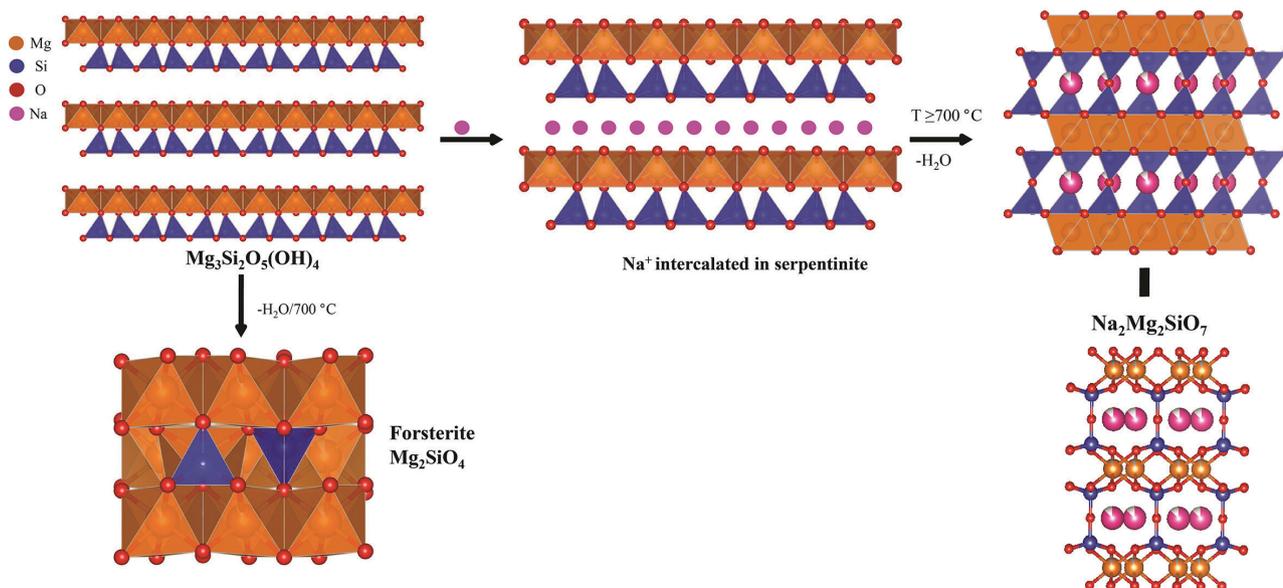
The forsterite structure resulted from the decomposition of the brucite ($Mg(OH)_2$) layer to form Mg−O−Si bonds. This structure crystallizes as orthorrombic system with space group P_{nma} where the (010) plan is composed of Mg-oxygen octahedra intercalated with [SiO_4]. In each tetrahedron [SiO_4] all the oxygen atoms are shared with Mg (Figure 3b). All structures were generated from the Crystallographic Information File (CIF) taken from the database, Crystallography Open Database[28] and generated from Vesta Visualization software for Electronic and Structure Analysis.[29]

The XRD (Figure 3) profiles of the samples $Serp_{700}$ and $5Na_{700}$ were very similar. On the other hand, the samples $10Na_{700}$ and $20Na_{700}$ showed a peak at ca. 21° suggesting the formation of the structure $Na_2Mg_2Si_2O_7$ (JCDPS 53-0626). In addition, a small peak at 43° indicates the formation of small amounts of MgO (JCDPS 45-946). These results suggest a process described by the simplified equation 2:

$$2NaOH + Mg_3Si_2O_5(OH)_4 \rightarrow Na_2Mg_2Si_2O_7/MgO + 3H_2O \quad (2)$$

XRD peaks related to forsterite gradually decreased in the presence of Na^+. A simple analysis of peak intensities of $Na_2Mg_2Si_2O_7$ ($2\theta = 21°$) and Mg_2SiO_4 ($2\theta = 32.5°$) phases suggests that the increase of sodium caused the ratio $I_{(Na_2Mg_2Si_2O_7)}/I_{(Mg_2SiO_2)}$ increase from 0.3 to 5.4 for the sample $20Na_{700}$. These results clearly indicate that the presence of Na^+ led to the formation of the phase $Na_2Mg_2Si_2O_7$. It is interesting to observe that the phase $Na_2Mg_2Si_2O_7$ has a Na:Mg:Si atomic ratio of 1:1:1, whereas the sample $20Na_{700}$ has a slightly different Na:Mg:Si ratio (1:1.2:0.8). The small excess of magnesium is segregated as MgO as indicated by the XRD pattern for the sample $20Na_{700}$.

The phase $Na_2Mg_2Si_2O_7$ crystallizes in a monoclinic system with space group Pc composed of sheets formed by [MgO_4] octahedra sheet connected by Si−O−Si bonds formed by Si_2O_7 units (Figure 4). The Na^+ species are located in the interlayer spaces, as shown in Figure 4. Considering the similarity between the layer structure and the Mg and Si distribution of the serpentinite and the
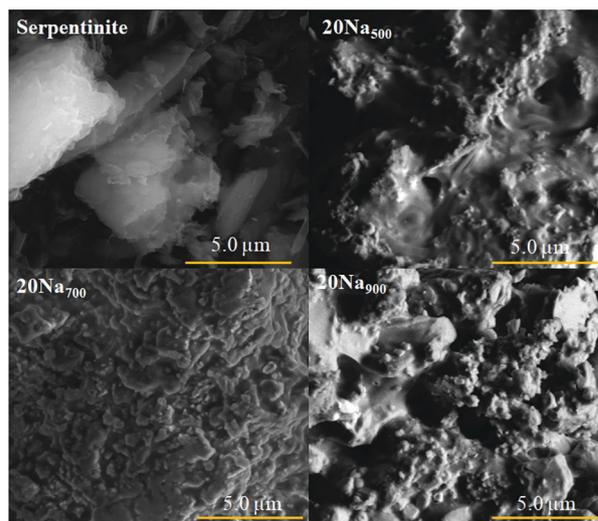

Figure 3. Structure of (a) serpentinite and (b) forsterite.

Figure 4. Representation of the reactions of serpentinite leading to forsterite (Mg_2SiO_4) and intercalation with Na^+ to produce the phase $Na_2Mg_2Si_2O_7$.

$Na_2Mg_2Si_2O_7$ structure, one may consider that the reaction pathway likely involves the diffusion/intercalation of Na^+ in the interlayer space of serpentinite, followed by a thermal decomposition to produce the phase $Na_2Mg_2Si_2O_7$. If the reaction is carried out in a different sequence, first treatment of serpentinite at 700 °C and only after this treatment impregnation with NaOH, then treatment again at 700 °C, no formation of the $Na_2Mg_2Si_2O_7$ phase was observed.

The effect of temperature on the sample 20Na was investigated at 500, 700 and 900 °C (see XRD in SI section). Pure serpentinite decomposes only at temperatures higher than 700 °C. However, in the presence of Na^+, the decomposition of serpentinite takes place at much a lower temperature, 500 °C, leading to the formation of the $Na_2Mg_2Si_2O_7$ and Na_2MgSiO_4 phase. As the treatment temperature increased to 700 and 900 °C the peaks related to the phase $Na_2Mg_2Si_2O_7$ increased in intensity.

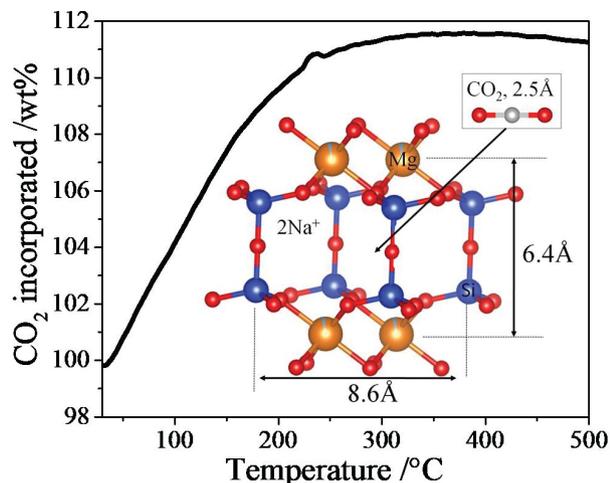SEM images for the serpentinite precursor (Figure 5) showed needle shaped fragmented particles with size varying from 1-10 μm. After impregnation with Na^+ and the thermal treatment a strong sintering takes place to form a solid with a compact surface. As a result of this sintering/compacting process, the surface decreased from 12 ($Serp_{700}$) to 8, 5 and 4 $m^2 g^{-1}$ for $20Na_{500}$, $20Na_{700}$ and $20Na_{900}$, respectively.

The CO_2 uptake by the sample $20Na_{700}$ was investigated by temperature programmed reaction experiments (Figure 6). It can be observed that the sample $20Na_{700}$ from ca. 50 up to 400 °C absorbed a relatively large amount of CO_2, ca. 12 wt.%, which indicates by a simple calculation a ratio of one CO_2 molecule for two Na^+ ions.

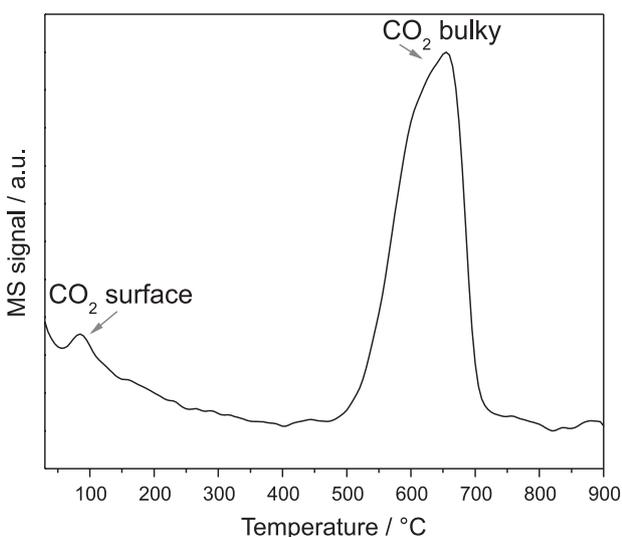**Figure 5.** SEM images of the samples serpentinite, $20Na_{500}$, $20Na_{700}$ and $20Na_{900}$.

This result suggests a strong basicity likely due to the presence of basic Na^+ species, which are available for the interaction with CO_2. The formation of carbonate species was investigated by Raman spectroscopy and XRD. Raman spectra of the obtained material did not show the typical absorption for CO_2 at 1381 cm^{-1} (SI section).[28] XRD of the $20Na_{700}$ sample after CO_2 reaction also did not show the presence of crystalline phases related to sodium carbonate and magnesium carbonate (SI section). It was only observed a general broadening and a shift of the peaks to lower 2θ of the XRD peaks suggesting that the $Na_2Mg_2Si_2O_7$ structure was not destroyed by CO_2 up to 900 °C. Although the exact physico-chemical process of CO_2 interaction with $Na_2Mg_2Si_2O_7$ is not clear, one can speculate that CO_2

Figure 6. Temperature programmed reaction of 20Na$_{700}$ with CO_2 (detail: dimensions of the Na$_2$Mg$_2$Si$_2$O$_7$ structural cavity and a CO_2 molecule).

molecules are diffusing into the solid structure Na$_2$Mg$_2$Si$_2$O$_7$ to interact with the basic sites. The Na$_2$Mg$_2$Si$_2$O$_7$ structure shows cavities with relatively large size, e.g., distances Si−Si 8.3 Å and Mg−Mg 6.4 Å, which could easily accommodate a CO_2 molecule with dimension of 2.5 Å. The detail in Figure 6 shows a schematic representation of a CO_2 molecule and the Na$_2$Mg$_2$Si$_2$O$_7$ cavity. However, more detailed studies are necessary to investigate the nature of the CO_2 interaction with Na$_2$Mg$_2$Si$_2$O$_7$.
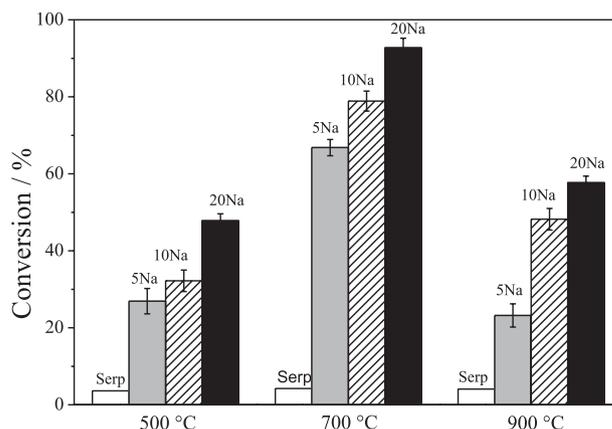
Temperature programmed desorption/decomposition was performed for samples 20Na$_{700}$ in a TG-MS system (Figure 7). The sample 20Na$_{700}$ showed a small desorption peak at ca. 80-90 °C, likely related to weak surface basic sites.[5] Another desorption process was observed at much higher temperature, 500-700 °C, related to the release of CO_2 molecules located in the Na$_2$Mg$_2$Si$_2$O$_7$ structure.

Figure 7. Temperature programmed CO_2 desorption of the sample 20Na$_{700}$ (after pretreatment at 500 °C under argon and exposure to CO_2 at 50 °C).

The different materials obtained by impregnation of 5, 10 and 20% sodium (Na$^+$) and treated at 500, 700 and 900 °C were tested as catalysts for the transesterification reaction of soybean oil in methanol (molar ratio of 1:9) using 5 wt.% catalyst at 60 and 100 °C. Blank tests (without catalyst) at 60 ºC showed no reaction, whereas at 100 ºC conversions lower than 5% were obtained.

The original serpentinite before and after treatment at 500-900 °C showed no significant activity for biodiesel production. On the other hand, materials impregnated with 5-20% Na$^+$ treated at 500 °C showed relatively low activities, i.e., up to 50% conversion. This result indicates that the Na$^+$ present in the sample is not fully active for the transesterification reaction. However, as the treatment temperature increased to 700 °C, the conversion improved significantly, reaching values higher than 90%. The sample treated at 900 °C showed a decrease on the catalytic activity (Figure 8).
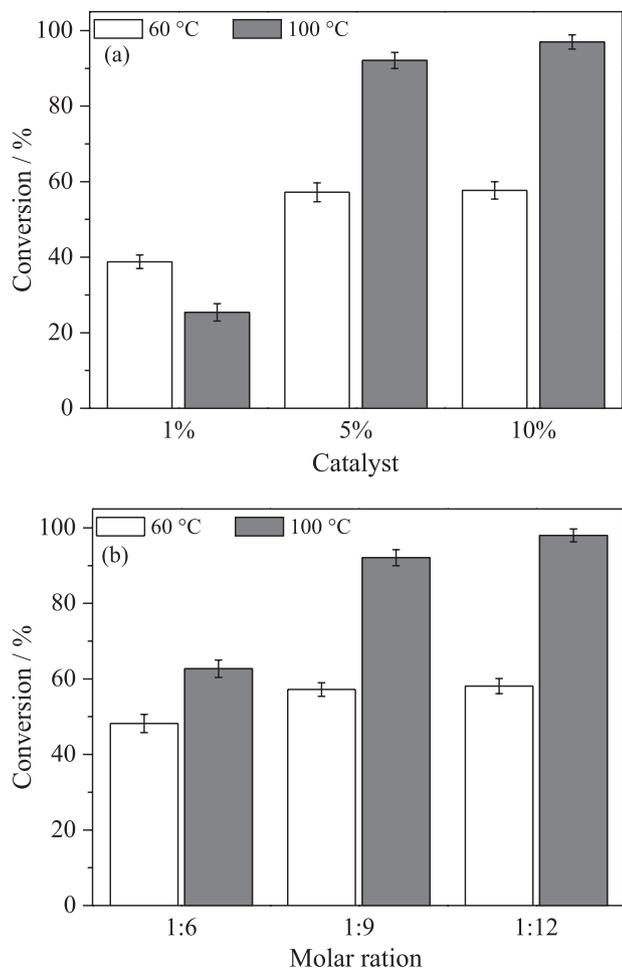

Figure 8. Transesterification results of soybean oil with methanol (molar ratio of 1:9, 5 wt.% catalyst at 100 °C for 3 h).

The transesterification kinetic was also investigated for the catalyst 20Na$_{700}$ and the obtained results are shown in SI section. These reactions were conducted in the molar ratio of 1:9, using 5% catalyst at temperatures of 60 and 100 °C. At 60 °C, the reaction reached equilibrium at ca. 60 min with maximum conversion of 55%. On the other hand, at 100 °C the conversion further increased to 95% reaching equilibrium at ca. 150 min.

The effects of the amount of catalyst as well as the different oil/alcohol molar ratios were evaluated and are presented in Figure 9. The tests were performed at 60 and 100 °C. The reaction time was 3 h.

Figure 9a data suggest the conversion of soybean oil to biodiesel improved when the amount of catalyst increased from 1 to 5 wt.%. On the other hand, when the catalyst amount increased to 10%, no significant change was observed, reaching 97% at 100 °C. The increase in
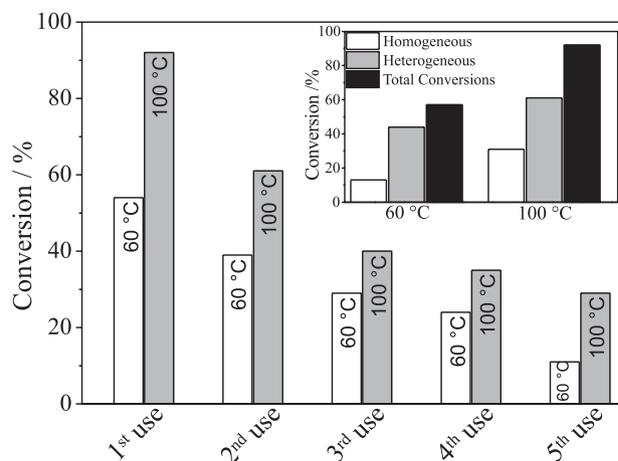
Figure 9. (a) Conversion (percentage) of 20Na$_{700}$ catalyst as a function of the amount of catalyst in the molar ratio of 1:9; (b) conversion of 20Na$_{700}$ catalyst as a function of different molar ratios using 5% catalyst.

the molar ratio (oil/methanol) from 1:6 to 1:9 led to an increase in the conversion, especially at 100 °C. However, the conversion did not vary significantly when the molar ration was further increased to 1:12 (Figure 9b).

The reuse of the catalyst was investigated using the 20Na$_{700}$ sample (Figure 10). After the first use, the conversion decreased from 92 to 63%. For the 3rd, 4th and 5th reactions the conversion slowly decreased reaching values ca. 30%.

The presence of Na$^+$ leaching and homogeneous reaction was investigated for the 20Na$_{700}$ catalyst mixed with methanol and heated to 60 or 100 °C and after 30 min the mixture was filtered hot and the methanol was used for the reaction with the soybean oil. These results were compared with a normal reaction with the catalyst 20Na$_{700}$ to separate the homogeneous and heterogeneous contributions. The results (Figure 10, detail) showed that the major contribution is heterogeneous (ca. 63% conversion at 100 °C), however, a significant leaching and homogeneous reaction is taking place (ca. 29% conversion at 100 °C).

The 2nd use showed a significant deactivation compared to the initial conversion, from 92 to 60% at 100 °C. After the 3rd use it was observed only a slight decrease on the catalytic activity. Preliminary results indicated that thermal treatment of the deactivated catalyst in air at 500-700 °C led to a partial recovery of the activity likely due to the elimination of organics from the catalyst surface. A more systematic work is necessary to understand the deactivation mechanism and possible reactivation processes.
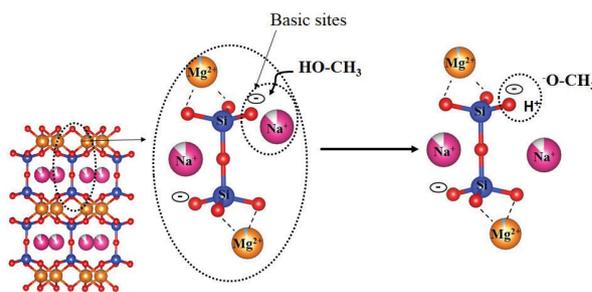

Figure 10. 20Na$_{700}$ reuse tests. Detail: conversion obtained during the leaching study.

Although the nature of the catalytic site is not clear, one can consider that in the Na$_2$Mg$_2$Si$_2$O$_7$ structure the Na$^+$ ions are interacting with one of the oxygens of the Si$_2$O$_7$ unit forming a basic species Si–O$^-$Na$^+$. One possible mechanism is the interaction of CH$_3$OH with the basic site Si–O$^-$Na$^+$ to form methoxide (equation 3).

$$Si–O^-Na^+ + CH_3OH \rightarrow Si–OH + Na^+ + CH_3O^- \qquad (3)$$

The formed methoxide is able to react with soybean ester to form biodiesel and regenerate the basic species.[29] A simplified local structure of the basic site and the reaction with methanol is represented schematically in Figure 11.

Figure 11. Schematic representation of the interaction of methanol molecule with the structural basic site Si–O$^-$Na$^+$.

Conclusions

The impregnation of serpentinite with NaOH and thermal treatment at temperatures 500-900 ºC led to the formation of the new phase $Na_2Mg_2Si_2O_7$. This reaction is discussed in terms of a diffusion and intercalation of Na^+ ions in the interlayer space of the serpentinite structure followed by dehydration. This phase $Na_2Mg_2Si_2O_7$ presented basic properties as observed by CO_2 temperature programmed reaction and desorption. The obtained materials showed catalytic activity for transesterification of soybean oil with methanol to produce biodiesel and were tested at 60 and 100 ºC. The catalytic site is discussed in terms of a Na^+ interacting with an Si_2O_7 moiety to form the basic species $Si-O^-Na^+$.

Supplementary Information

Supplementary data (TG/DTG, XRD, Raman spectra and kinetic data of the $20Na_{700}$ catalysts) are available free of charge at http://jbcs.sbq.org.br as PDF file.

Acknowledgments

References

1. Yoo, K.; Kim, B.-S.; Kim, M.-S.; Lee, J.; Jeong, J.; *Mater. Trans.* **2009**, *50*, 1225.

2. Dlugogorski, B. Z.; Balucan, R. D.; *Renewable Sustainable Energy Rev.* **2014**, *31*, 353.

3. Hirth, G.; Guillot, S.; *Elements* **2013**, *9*, 107.

4. Cao, C. Y.; Liang, C. H.; Yin, Y.; Du, L. Y.; *J. Hazard. Mater.* **2017**, *329*, 222.

5. Ballotin, F. C.; Cibaka, T. E.; Ribeiro-Santos, T. A.; Santos, E. M.; Teixeira, A. P. C.; Lago, R. M.; *J. Mol. Catal. A: Chem.* **2016**, *422*, 258.

6. Teixeira, A. P. C.; Santos, E. M.; Vieira, A. F. P.; Lago, R. M.; *Chem. Eng. J.* **2013**, *232*, 104.

7. Dollase, W. A.; *Powder Diffr.* **1996**, *11*, 51.

8. Xia, Y.; Chen, J.; Liu, Y.-G.; Mei, L.; Huang, Z.; Fang, M.; *Mater. Express* **2016**, *6*, 37.

9. Shen, X.; Wang, Y.; Ahring, B. K.; Lei, H.; Gao, Q.; Liu, H.; *RSC Adv.* **2015**, *5*, 96990.

10. Qian, K.; Shen, X.; Wang, Y.; Gao, Q.; Ding, H.; *Energy* **2015**, *93*, 2251.

11. Devi, K. B.; Lee, B.; Roy, A.; Kumta, P. N.; Roy, M.; *Mater. Lett.* **2017**, *207*, 100.

12. Ghods, B.; Meshkani, F.; Rezaei, M.; *Int. J. Hydrogen Energy* **2016**, *41*, 22913.

13. Ornar, A. A.; *Ceram. Int.* **1990**, *16*, 47.

14. Wang, J.; Yang, L.; Luo, W.; Yang, G.; Miao, C.; Fu, J.; Xing, S.; Fan, P.; Lv, P.; Wang, Z.; *Fuel* **2017**, *196*, 306.

15. Jia, Y.; Qiao, H.; Zheng, Y.; Guo, N.; You, H.; *Phys. Chem. Chem. Phys.* **2012**, *14*, 3537.

16. Teo, S. H.; Rashid, U.; Thomas Choong, S. Y.; Taufiq-Yap, Y. H.; *Energy Convers. Manage.* **2017**, *141*, 20.

17. Fan, M.; Liu, Y.; Zhang, P.; Jiang, P.; *Fuel Process. Technol.* **2016**, *149*, 163.

18. Tubino, M.; Rocha, J. G.; Bauerfeldt, G. F.; *Catal. Commun.* **2016**, *75*, 6.

19. Santório, R.; Veloso, C. O.; Henriques, C. A.; *J. Mol. Catal. A: Chem.* **2016**, *422*, 234.

20. Veiga, P. M.; Veloso, C. O.; Henriques, C. A.; *Renewable Energy* **2016**, *99*, 543.

21. Santiago-Torres, N.; Romero-Ibarra, I. C.; Pfeiffer, H.; *Fuel Process. Technol.* **2014**, *120*, 34.

22. Manadee, S.; Sophiphun, O.; Osakoo, N.; Supamathanon, N.; Kidkhunthod, P.; Chanlek, N.; Wittayakun, J.; Prayoonpokarach, S.; *Fuel Process. Technol.* **2017**, *156*, 62.

23. Al-Ani, A.; Darton, R. J.; Sneddon, S.; Zholobenko, V.; *ACS Appl. Nano Mater.* **2018**, *1*, 310.

24. Martínez, S. L.; Romero, R.; Natividad, R.; González, J.; *Catal. Today* **2014**, *220-222*, 12.

25. Xu, J.; Chen, T.; Shang, J. K.; Long, K. Z.; Li, Y. X.; *Microporous Mesoporous Mater.* **2015**, *211*, 105.

26. Barakos, N.; Pasias, S.; Papayannakos, N.; *Bioresour. Technol.* **2008**, *99*, 5037.

27. Guzmàn-Vargas, A.; Santos-Gutérrez, T.; Lima, E.; Flores-Moreno, J. L.; Oliver-Tolentino, M. A.; Martínez-Ortiz, M. D. J.; *J. Alloys Compd.* **2015**, *643*, S159.

28. Chen, Y.; Wang, H.; Li, J.; Lockard, J. V.; *J. Mater. Chem. A* **2015**, *3*, 4945.

29. Cordeiro, C. S.; da Silva, F. R.; Wypych, F.; Ramos, L. P.; *Quim. Nova* **2011**, *34*, 477.